Quantitative measurement of displacement and strain by the numerical moiré method

Chunwang Zhao (赵春旺)[1], Yongming Xing (邢永明)[1], Pucun Bai (白朴存)[2], and Lifu Wang (王利福)[1]

[1] *College of Science, Inner Mongolia University of Technology, Hohhot 010051*

[2] *College of Materials Science and Engineering, Inner Mongolia University of Technology, Hohhot 010051*

Received October 22, 2007

The numerical moiré method with sensitivity as high as 0.03 nm has been presented. A quantitative displacement and strain analysis program has been proposed by using this method. It is applied to an edge dislocation and a stacking fault in aluminum. The measured strain of edge dislocation is compared with theoretical prediction given by Peierls-Nabarro dislocation model. The displacement of stacking fault is also obtained.

OCIS codes: 070.1170, 120.2650, 120.3940.

Moiré method was introduced by Weller *et al.*[1] in 1948 and has been improved by many researchers. The classical moiré method, referred to as geometric or mechanical moiré method, has been widely used in experimental stress analysis. It is a full-field optical method used to measure in-plane deformation. The measurement sensitivity for displacement using the moiré method is decided upon by the pitch of the specimen grid. The grid fabrication techniques employed for the geometrical coarse moiré method have been well developed. Since the 1980s, holographic techniques have been used to produce laser moiré interferometry gratings. The displacement sensitivity of this method is about 300 nm[2]. Moiré interferometry has had a wider application and development[3]. The three-dimensional (3D) displacement can also be measured[4]. The electron moiré method was developed by Kishimoto *et al.* in 1991[5], and then advocated by Dally *et al.*[6]. The displacement sensitivity of this method is about 100 nm. With the development of nanotechnology, transmission electronic microscopy (TEM) has been widely used for analysis and measurement in mechanics and materials science. Moiré fringes in TEM image were first used by Menter[7] to identify a dislocation. Later, the moiré pattern was thought of as a magnified view of the structure of materials. Such patterns can be used to locate and give information about the dislocation if it is associated with a terminating lattice plane in one material, but we do not actually see the dislocation. In TEM, the moiré fringes can be explained by double diffraction corresponding to interference between a pair of electronic beams, g_1 and g_2[8]. Dai *et al.*[9,10] proposed a nano-moiré method with the TEM image. In their experiment, a crystal lattice was utilized as a specimen grating, while a prepared unidirectional geometric grating was used as reference grating. These two gratings interfered to generate a nano-moiré fringe. Dislocation of Peierls type and the deformation field could then be detected. The displacement sensitivity of this method can reach 1 nm.

In this paper, we present a nano-scale measurement method, numerical moiré (NM) method, whose sensitivity can reach 0.03 nm. The method we use is an extension of a technique firstly developed in optical interferometry[11], and later utilized for the study of defects[12,13]. We propose a quantitative analysis program and apply the program to an edge dislocation and a stacking fault.

An image of the atomic lattice is obtained via high-resolution transmission electron microscopy (HRTEM), and lattice fringes are created by the interference of diffracted beams with the transmitted beam. All the information contained in a HRTEM image can be obtained by analyzing these few components of the image intensity. The lattice fringes seen in the image are related to the atomic planes in the specimen. Figure 1 shows a typical image with its decomposition into different lattice fringes of silicon. The crossing of the different fringes produces the dot-like contrast corresponding to the atomic columns viewed in [111] projection. The displacement and strain can be obtained by the measurement of these atomic column positions. An image of a perfect crystal

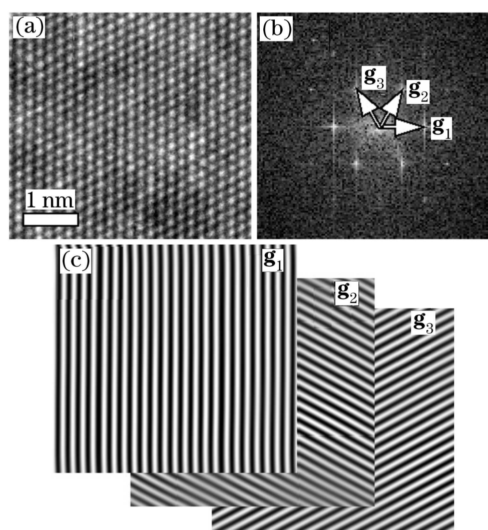

Fig. 1. Lattice fringe images. (a) Typical HRTEM image of the atomic lattice in [111] projection of silicon; (b) Fourier transform of HRTEM image; (c) individual lattice images corresponding to the planes $(20\bar{2})$, $(02\bar{2})$, and $(\bar{2}20)$ respectively.

 © 2008 Chinese Optics Letters

can be described as a Fourier series:

$$I(\mathbf{r}) = \sum_{\mathbf{g}} A_g \mathrm{e}^{2\pi i \mathbf{g}\cdot\mathbf{r}}, \quad (1)$$

where $I(\mathbf{r})$ is the intensity in the image at position $\mathbf{r}$, A_g are the Fourier coefficients, $\mathbf{g}$ represents the periodicities corresponding to the Bragg reflections and has the following relationship with the lattices fringe spacing d:

$$d = \frac{1}{|\mathbf{g}|}. \quad (2)$$

To describe the variations of contrast and fringe position in the image, we allow the Fourier components, A_g, to become a function of position $\mathbf{r}$:

$$I(\mathbf{r}) = \sum_{\mathbf{g}} A_g(\mathbf{r}) \mathrm{e}^{2\pi i \mathbf{g}\cdot\mathbf{r}}. \quad (3)$$

The image of a particular set of lattice fringes $I_g(\mathbf{r})$ is therefore given by

$$I_g(\mathbf{r}) = A_g(\mathbf{r}) \mathrm{e}^{2\pi i \mathbf{g}\cdot\mathbf{r}}. \quad (4)$$

Let us assume that there is a displacement $\mathbf{u}(\mathbf{r})$,

$$\mathbf{r} \rightarrow \mathbf{r} - \mathbf{u}(\mathbf{r}), \quad (5)$$

then Eq. (4) becomes

$$I'_g(\mathbf{r}) = A_g(\mathbf{r}) \mathrm{e}^{2\pi i \mathbf{g}\cdot\{\mathbf{r}-\mathbf{u}(\mathbf{r})\}}, \quad (6)$$

where the amplitude, $A_g(\mathbf{r})$, describes the local contrast of the fringes. $2\pi\mathbf{g}\cdot\{\mathbf{r}-\mathbf{u}(\mathbf{r})\}$ is a geometric phase and describes the position of the fringes. Introducing a magnification M and calculating a new phase

$$P'_g(\mathbf{r}) = 2\pi\frac{\mathbf{g}\cdot\mathbf{r}}{M} - 2\pi\mathbf{g}\cdot\mathbf{u}(\mathbf{r}), \quad (7)$$

the NM can be attained by calculating the cosine of the resulting phase,

$$I_g^{\text{moiré}}(\mathbf{r}) = \cos\{2\pi\frac{\mathbf{g}}{M}\cdot\mathbf{r} - 2\pi\mathbf{g}\cdot\mathbf{u}(\mathbf{r})\}. \quad (8)$$

This is equivalent to superimposing a perfect lattice with a reciprocal lattice vector smaller than the average lattice by a factor of $1-\frac{1}{M}$. The NM pattern acts as a lens which magnifies not only the lattice spacing (by a factor of M) but also the distortions and rotations (by the same factor M). The method produces a map of the local fringe contrast and the displacements of the lattice with respect to a perfect reference lattice. The displacement, $\mathbf{u}(\mathbf{r})$, in the direction of the reciprocal lattice vector, $\mathbf{g}$, will therefore be given by

$$\mathbf{u}_g(\mathbf{r}) = \frac{\mathbf{r}-\mathbf{r}_0}{M}. \quad (9)$$

By combining the information from two sets of lattice fringes, the in-plane displacement field can be calculated (provided that the reciprocal lattice vectors, $\mathbf{u}_{g1}$ and $\mathbf{u}_{g2}$ are non-colinear). The strain can be calculated by the measurement of the spacing between moiré fringes. Assuming that the spacing of undistorted lattice is D and the spacing of the distorted lattice is D', then the strain $\varepsilon_g(\mathbf{r})$ in the direction of the reciprocal lattice vector will be given by

$$\varepsilon_g = \frac{D'-D}{D}. \quad (10)$$

By combining the information from two sets of lattice fringes, the in-plane strain field can be calculated.

A verification of the technique can be achieved with the following example. Figure 2(a) is a calculation for a cosine lattice fringe with a spacing of 2 nm. There is a displacement of 0.2 nm at the areas marked by the arrows. At first, the Fourier transform image is calculated, as shown in Fig. 2(b). Then the right diffraction spot is selected for filtering by a Gaussian mask. The magnification is 5. This can be carried out by changing the reference to 0.8$\mathbf{g}$ followed by an inverse Fourier transform that produces a complex image containing the desired information. The geometric phase can be obtained by calculating the arctangent of the imaginary part divided by the real part, point by point in the image. At last, the NM can be obtained by calculating the cosine of the resulting phase image, Fig. 2(c). According to Eq. (9), the local displacement $\mathbf{u}(\mathbf{r})$ can be obtained by measuring the distance between the peaks of distorted fringes and undistorted fringes, as shown in Fig. 2(d). There is a displacement of 0.2 nm in the range of $10-20$ nm. According to Eq. (10), the local strain $\varepsilon(\mathbf{r})$ can be obtained by measuring the spacing between the peaks of moiré fringes, as shown in Fig. 2(e). There are a strain of -0.1 near 10 nm and a strain of $+0.1$ near 20 nm. The reliable measurement result has verified the NM technique.

The TEM experimental material was aluminum whose Poisson's ratio was $\nu = 0.347$ and lattice constant $d_{111} = 0.2338$ nm. The TEM sample was prepared for cross sectional imaging along the $[\bar{1}10]$ direction using standard techniques involving mechanical grinding followed by ion milling. A HRTEM experiment was performed on the

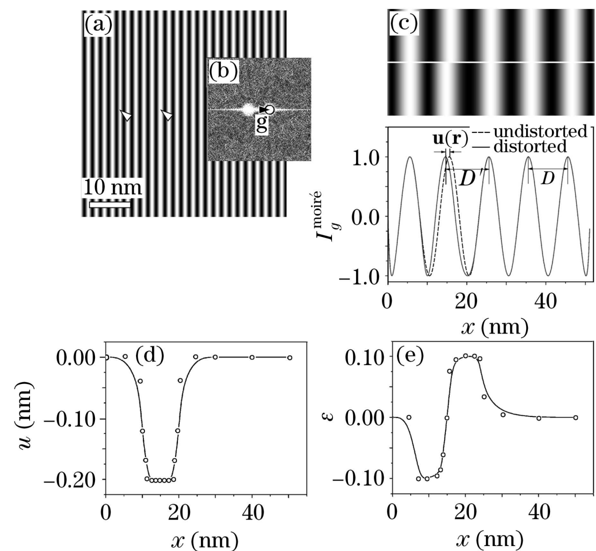

Fig. 2. Verification of the technique. (a) Calculated fringe image with a displacement of 0.2 nm; (b) Fourier transform of fringe image; (c) 5× NM image; (d) displacement measurement result; (e) strain measurement result.

JEM-2010 operating at 200 kV. Images were recorded on a 1024×1024 pixels slow scan charge-coupled device (CCD) camera (Gatan 794), and the image analysis was carried out using a software package developed with the Gatan Digital Micrograph environment.

A HRTEM image of an edge dislocation in aluminum is shown in Fig. 3(a). The dislocation core is marked by an arrow. The (111) spot in the Fourier transform of the image (Fig. 3(b)) was chosen for analysis. A mask was placed around the spot to isolate it, and the NM image was calculated (Fig. 3(c)). The magnification in this image is 5. The spacing was nearly constant in the area away from dislocation core, which was used as the reference. Taking the x axis parallel to the $\mathbf{g}_{111}$ orientation and the y axis in the perpendicular direction, the Cartesian coordinate system can be established. The resulting fringe patterns can then be binarized (Fig. 3(d)). The strain component ε_{xx} can be calculated by measuring the spacing between the fringes. The size of Fig. 3(a) is 456×205 pixels. The size of one pixel is 0.0352×0.0352 (nm). So the error of the displacement measurement is one pixel (0.0352 nm). Considering that the space between two binarized fringes is $(0.2338 \times 5/2 =)0.5845$ nm, the error of the strain measurement is $0.0352/0.5845 = 0.06$.

The strain distribution from the experimental results is then compared with that from the Peierls-Nabarro dislocation model. According to the Peierls-Nabarro dislocation model, the strain of an edge dislocation along the x direction can be written as

$$\varepsilon_{xx} = -\frac{d}{\pi}\frac{(1-\nu)y}{4(1-\nu)^2x^2+y^2}, \tag{11}$$

where x and y are the Cartesian coordinates, respectively, centered on the dislocation core position, d is the lattice constant along x direction, and ν is Poisson's ratio. The strain results of the experiment and theoretical prediction are shown in Fig. 4. A good agreement can be found except for the region with a distance less than 1 nm from the dislocation core. Within the 1-nm range, the measurement strain is somewhat higher than the theoretical prediction. The strain at the dislocation core can reach 0.47 ± 0.06.

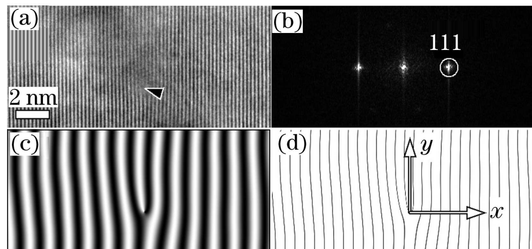

Fig. 3. NM analysis of edge dislocation in aluminum. (a) HRTEM image; (b) Fourier transform of HRTEM image; (c) 5× NM image; (d) binarized moiré image.

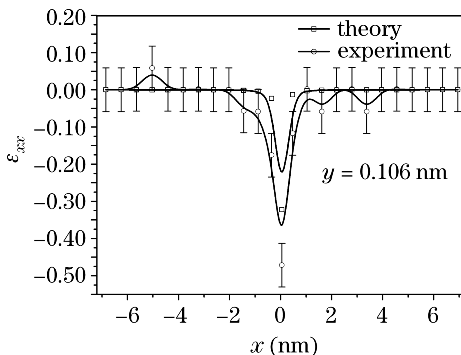

Fig. 4. Comparison of strain ε_{xx} between the experimental result and theoretical prediction.

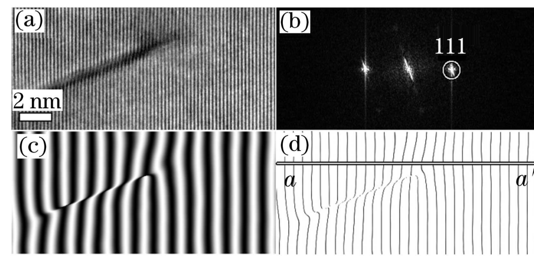

Fig. 5. NM analysis of stacking fault in aluminum. (a) HRTEM image; (b) Fourier transform of HRTEM image; (c) 5× NM image; (d) binarized moiré image.

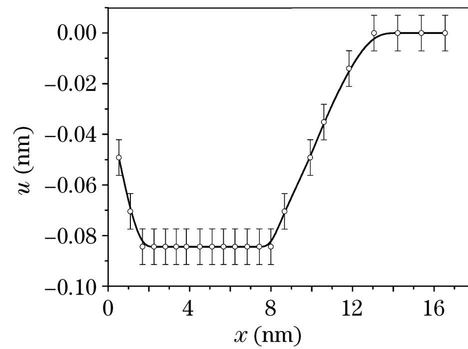

Fig. 6. Displacement near the stacking fault.

A HRTEM image of a stacking fault in aluminum is shown in Fig. 5(a). The (111) spot in the Fourier transform of the image (Fig. 5(b)) was chosen for analysis. A mask was placed around the spot to isolate it and the NM image was calculated (Fig. 5(c)). The magnification is 5. The spacing was nearly constant on the bottom of image, which was used as the reference. The resulting fringe patterns can then be binarized (Fig. 5(d)). The displacement u along the section aa' in Fig. 5(d) is shown in Fig. 6. The maximum is 0.084 ± 0.007 nm.

In this paper, the theory of NM is presented in detail. The technique is verified by a set of fringes of known distortion. This technique has been applied to an edge dislocation and a stacking fault in aluminum. The displacement sensitivity of NM is 0.0352 nm in our experiment, corresponding to the 1000000× magnification of HRTEM. The displacement sensitivity can be increased by increasing the magnification of the HRTEM. Using CCD with higher resolution, e.g. 2048×2048 pixels, the displacement sensitivity will be increased to 0.0176 nm.

This work was supported by the National Natural Science Foundation of China under Grants No. 10562003 and 10272054. C. Zhao's e-mail address is zhaocw@imut.edu.cn.

References

1. R. Weller and B. M. Shephard, Proc. Soc. Exp. Stress Anal. **6,** 35 (1948).
2. D. Post, in *Mechanics of Nondestructive Testing* W. W. Stinchcomb, (ed.) (Plenum Press, New York, 1980) pp.197 − 216.
3. J. Hu, A. Zeng, and X. Wang, Chin. Opt. Lett. **4,** 18 (2006).
4. W. Wang and J. Sun, Chin. Opt. Lett. **2,** 396 (2004).
5. S. Kishimoto, M. Egashira, N. Shinya, and R. A. Carolan, in *Proceedings of the 6th Int. Conf. Mech. Behavior of Materials* **4,** 661 (1991).
6. J. W. Dally and D. T. Read, Exp. Mech. **33,** 270 (1993).
7. J. W. Menter, Proc. Roy. Soc. Lond. A **236,** 119 (1956).
8. D. B. Williams and C. B. Carter, *Transmission Electron Microscopy: A Textbook for Materials Science* (Plenum Press, New York, 1996).
9. F. L. Dai and Y. M. Xing, Acta Mech. Sin. **15,** 283 (1999).
10. Y. M. Xing, F. L. Dai, and W. Yang, Sci. China Ser. A **43,** 963 (2000).
11. M. Takeda, H. Ina, and S. Kobayashi, J. Opt. Soc. Am. **72,** 156 (1982).
12. M. Takeda and J. Suzuki, J. Opt. Soc. Am. A **13,** 1495 (1996).
13. S. Zghal, M. J. Hÿtch, J.-P. Chevalier, R. Twesten, F. Wu, and P. Bellon, Acta Mater. **50,** 4695 (2002).